PHYSICAL REVIEW B **86**, 125309 (2012)

Dielectric response of epitaxially strained $CoFe_2O_4$ spinel thin films

Diego Gutiérrez, Michael Foerster,[*] Ignasi Fina, and Josep Fontcuberta
Institut de Ciència de Materials de Barcelona (ICMAB-CSIC), Campus UAB, Bellaterra 08193, Catalonia, Spain

Daniel Fritsch
H. H. Wills Physics Laboratory, University of Bristol, Tyndall Avenue, Bristol BS8 1TL, United Kingdom

Claude Ederer
Materials Theory, ETH Zürich, Wolfgang-Pauli-Straße 27, CH-8093 Zürich, Switzerland

(Received 12 June 2012; published 10 September 2012)

Aiming to explore strain effects on the dielectric permittivity of ultrathin films of oxides with spinel structure, we report here on the thickness (4–160 nm) dependence of the dielectric response of $CoFe_2O_4$ (CFO) epitaxial films grown on $La_{2/3}Sr_{1/3}MnO_3$ buffered $SrTiO_3(001)$ substrates. It is found that films thicker than ~30 nm display bulklike permittivity values ($\varepsilon_r \approx 14$); however, a pronounced and gradual ε_r reduction is observed for thinner films when the in-plane compressive strain induced by the substrate increases. First-principle calculations are used to simulate the variation of the permittivity of CFO spinel thin films under epitaxial strain; in agreement with simple bond-length considerations, the out-of-plane permittivity is predicted to increase under in-plane compressive strain due to the resulting out-of-plane lattice expansion, but this enhancement can be overcompensated if this expansion is suppressed, resulting in an effective reduction of permittivity. However, the predicted reduction is substantially smaller than observed experimentally. We discuss possible mechanisms to account for this observation.

DOI: 10.1103/PhysRevB.86.125309 PACS number(s): 77.80.bn, 77.55.F−, 77.55.Bh

I. INTRODUCTION

Materials having spinel AB_2X_4 structures are receiving renewed attention. One reason for this interest is that their properties can be easily tuned because of the complex anion-cation bond network which forms and connects the octahedral (B) and tetrahedral (A) sublattices, and the ability of the structure to admit a large variety of ions at A, B, and X sites. Moreover, when magnetic cations are involved, competing magnetic interactions within and between each sublattice, together with the fact that the B-cations tetrahedral network implies the existence of topological magnetic frustration, lets one anticipate a strong impact of the structural composition/details on the magnetic properties. In the last few years, a number of uncommon phenomena, ranging from heavy fermions[1] to the rare coexistence of ferroelectricity and ferromagnetism[2,3] or the existence of negative thermal expansion[4] have been discovered in materials from the spinel family, illustrating that in this structure the complex equilibrium between spin, charge, orbitals, and the lattice rivals with that of the better known perovskites. These discoveries are of fundamental interest but they may also lead to new applications. For example, the integration of ferromagnetic insulating spinels in magnetic tunnel junctions has been proposed as a method to obtain fully spin-polarized current sources,[5–7] while the integration of multiferroic spinels in tunnel junctions could lead to advanced spintronic components as explored for perovskite oxides.[8]

Whereas the structural, thermal, optical, and magnetic properties of bulk spinels are rather well known, the properties of spinel thin films have received much less attention. Moreover, the powerful route to tailor unit-cell dimensions by substrate-induced epitaxial strain, which has been much exploited in some oxides (i.e. binary and perovskites), has been less explored in spinel thin films. The recognition that the spinel structure is very open [only a fraction of the tetrahedral (1/4) and octahedral (1/2) sites within the anionic scaffold are actually occupied by cations] suggests that strain can be accommodated in intricate ways, thus leaving opportunities for emerging properties. Indeed, it has been recently shown that epitaxial strain effects in Fe[CoFe]O_4 (CFO), a prototypical ferrimagnetic spinel, are very subtle, and when increasing stress the unit cell deforms without preserving the unit-cell volume, thus implying potentially severe bond distortions and subsequent changes in the lattice dynamics and functional properties.[9,10]

Some effects of epitaxial strain on the properties of magnetic spinels, most notably CFO, have been investigated.[11–18] It is interesting to note that in perovskites, the influence of epitaxial strain on the dielectric properties is well known and has led to breakthrough discoveries such as induced or enhanced ferroelectricity,[19] metal-insulator transitions,[20] coexisting ferroelectric and ferromagnetic orders,[21] or fine tuning of complex antiferromagnetic orders.[22] However, in the case of spinel thin films these effects have only received little attention.[23]

Here we address this issue by exploring the dielectric response of epitaxial CFO films in different compressive strain states. These states are realized by epitaxial growth of CFO on a suitable substrate/buffer layer and gradual relaxation of the film upon increasing thickness from 4 to 160 nm. It turns out that the films thicker than ~30 nm display bulk-like permittivity values ($\varepsilon_r \approx 14$); however, a clear, gradual reduction of ε_r is observed for increasing substrate-induced compressive in-plane strain for thicknesses below 30 nm. We discuss possible mechanisms to account for this result.

II. EXPERIMENT

Samples were prepared by pulsed laser deposition on (001) $SrTiO_3$ (STO) single-crystalline substrates using a KrF laser. First, a metallic $La_{2/3}Sr_{1/3}MnO_3$ (LSMO) bottom electrode of thickness $d_{LSMO} \approx 25$ nm was deposited and a thin CFO dielectric layer of thickness d was subsequently grown on top. The thicknesses of CFO (d) and LSMO (d_{LSMO}) were determined by x-ray reflectometry (XRR) and found to agree with the number of laser pulses after appropriate CFO and LSMO growth-rate calibrations. The CFO films reported here have thicknesses of 160, 67, 50, 25, 17, 8.5, and 4.2 nm. CFO films were grown using 1.6 J cm^{-2} laser fluence, a repetition rate of 5 Hz at 500 °C, and oxygen pressure of 0.1 mbar. After growth the films were *in situ* annealed at 450 °C for 60 min under 200 mbar of oxygen. The growth rate of CFO is $\sim$2 nm/min.

Bulk STO, LSMO, and CFO can be described using cubic unit cells of parameters: a(STO) = 3.905 Å, a(LSMO) = 3.873 Å, and a(CFO) = 8.392 Å, respectively. Consequently, it is expected that the substrate and buffer layer will induce an in-plane compressive strain on the CFO film.

X-ray diffraction (XRD) experiments using Cu $K\alpha$ radiation were performed using a Rigaku Rotaflex 200B diffractometer for $\theta/2\theta$ scans; reciprocal space maps were collected using a Bruker 1T8 Advance diffractometer equipped with a bidimensional detector; and grazing incidence XRD (GIXRD) using a MRD X'Pert Pro (Panalytical, Almelo). The CFO layers were characterized (topography and current maps) with a Nanotec Cervantes atomic force microscope (AFM) equipped with Nanosensor CDT-NCHR conductive tips (boron doped diamond coating). The topography images confirmed the homogeneity and low roughness (from $\sim$0.2 nm for the 4.2-nm CFO layer to 2 nm for 50 nm), while no visible hot spots were detected in current maps.

Two different types of circular electric contacts were used: (a) Pt contacts (with diameters from 490 μm to 112 μm) and (b) Au contacts (with diameters from 490 μm to 5.9 μm). Pt and Au contacts (with diameters larger than 112 μm) were deposited by sputtering through suitable masks. On the other hand, we also used smaller (diameter <112 μm) Au contacts made by electron beam lithography. The use of smaller contact areas in such ultrathin films reduces the probability to encounter short circuits or large leakage currents in the contact region. These latter contacts were made by first sputtering a thin Au layer on the CFO and an e-beam lithography step using polymethyl methacrylate (PMMA) as resist. In exposed areas, the Au was removed by wet etching; removing the residual resin from nonirradiated areas thus left the Au contacts accessible. By using this method, Au contacts with areas A from 88 μm^2 to 28 μm^2 were fabricated, where A was measured by scanning electron microscopy (SEM).

The contacts having areas smaller than 85 μm^2 were electrically connected by using a modified setup of the AFM. The conducting AFM tip was connected, via a coaxial wire, to one input channel of an Agilent 4192A LF impedance analyzer, while the second input was connected to the LSMO bottom electrode. The impedance was measured by using an ac-driving voltage ($V_{ac} = 200$ mV) at frequencies (f) within the 100 Hz–1 MHz range. When appropriate, a bias dc voltage (V_{dc}) was applied. The sample holder and the whole AFM setup were connected to the ground of the impedance analyzer.

III. COMPUTATION

The dielectric permittivity of CFO is calculated using density functional perturbation theory[24] as implemented in the Vienna *ab initio* Simulation Package (VASP).[25] Thereby, the inverse spinel structure is represented by a low-energy cation arrangement with $P4_122$ symmetry, containing four formula units per cell (see Refs. 26 and 27). We use standard projector-augmented wave potentials including nine valence electrons per Co, 14 valence electrons per Fe, and six per O. A plane wave energy cutoff of 500 eV and a Γ-centered $5 \times 5 \times 3$ k-point mesh ensure sufficient accuracy of our calculations. The generalized gradient approximation of Perdew, Burke, and Ernzerhof[28] in combination with the Hubbard "$+U$" correction,[29] where $U = 3$ eV and $J = 0$ eV, which is applied to both Fe and Co d states, is used for the exchange-correlation energy. To simulate the effect of epitaxial strain we constrain the "in-plane" and "out-of-plane" lattice constants to different values while fully relaxing all ionic positions until the forces are smaller than 5×10^{-5} eV/Å.

IV. RESULTS AND DISCUSSION

X-ray diffraction patterns in $\theta/2\theta$ scans show only the (00l) reflections of CFO, LSMO, and STO, indicating a textured growth along the c axis for both layers. In Fig. 1(a) we show a region of the $\theta/2\theta$ scan where the (004) reflection of CFO appears for a number of films of various thicknesses. Inspection of this image reveals a gradual shift of the (004) reflection towards lower angles when reducing film thickness. This indicates an expansion of the out-of-plane c parameter when reducing thickness, as expected for an in-plane compressed film. We note in Fig. 1(a) that the c axis of the 67-nm film is still larger than bulk CFO (dashed line) reflecting the presence of a minor strain. In contrast, the 160-nm film was found to be fully relaxed. The c-axis unit-cell lengths evaluated from these $\theta/2\theta$ plots, shown in Fig. 1(c), illustrate the gradual expansion of the c axis for $d \leqslant 67$ nm. A very similar trend had been found for CFO films grown on bare STO substrates.[10]

In Fig. 1(b) we show GIXRD of the thinnest films in the angular region where the (440) reflection of CFO occurs. The vertical dashed line indicates the position of the corresponding reflection of bulk CFO. Data in Fig. 1(b) clearly shows that the (440) reflections of these ultrathin films are shifted towards larger 2θ angles than bulk CFO when reducing thickness, thus reflecting an enhanced in-plane compression. Therefore, data in Figs. 1(a) and 1(b) clearly show that CFO films on LSMO/STO(001) are in-plane compressed and gradually relax towards bulk value when increasing thickness d (in round brackets): a(4.2 nm) = 8.255 Å, a(8.5 nm) = 8.322 Å, a(50 nm) = 8.361 Å, and a(67 nm) = 8.382 Å. Within the experimental accuracy, the reciprocal space maps lead to similar (a,c) cell parameters. As shown in Fig. 1(a), the position of the LSMO reflections of all films remains fixed and indicates a fully coherent growth of LSMO on STO.

The dependence of the capacitance on the ac frequency $C(f)$ for the thickest CFO film (160 nm) is shown in Fig. 2

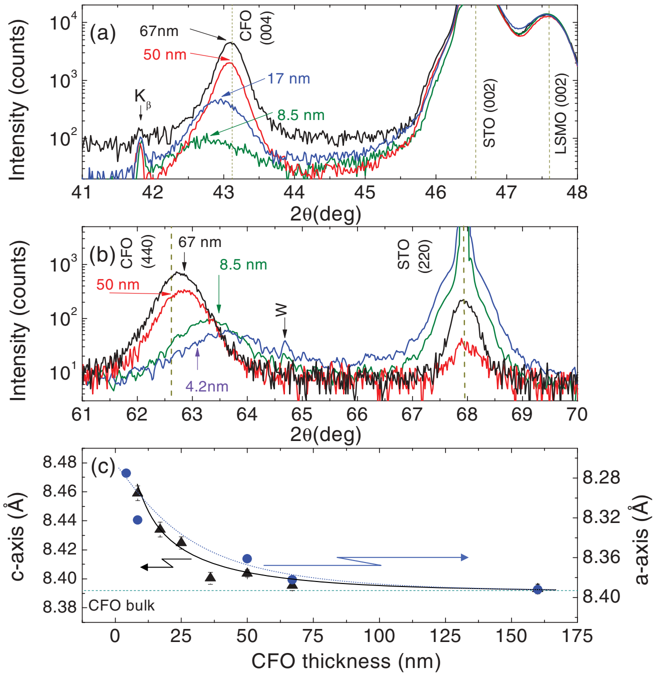

FIG. 1. (Color online) (a) $\theta/2\theta$ XRD scans around symmetric reflections of the CFO/LSMO//STO(001) heterostructures for different CFO thicknesses; dashed lines indicate the position of bulk (004) CFO and (002) STO and the position of the (002) reflection of LSMO bottom layer. The reflection of tungsten (W) comes from the equipment. (b) GIXRD patterns around the (440) CFO reflection of some CFO/LSMO//STO(001) heterostructures; dashed lines indicate the position of the corresponding bulk reflections of (440) CFO and (220) STO. (c) Thickness dependence of the out-of-plane (left axis) and in-plane (right axis) parameters of CFO films, extracted from fits to the data in (a), using a Gaussian profile. Dashed line indicate the unit-cell volume of bulk CFO.

(contact area 9800 μm^2). In Fig. 2 we include data obtained using Pt contacts under different V_{dc} bias conditions. The first observation is that for $V_{dc} = 0$, the capacitance displays two well-defined regions: a low-f region of high capacitance and a high-f region of smaller capacitance, weakly depending on frequency. In Fig. 2 (right axis) we show the corresponding permittivity (ε^*) calculated using $C = \varepsilon_0 \varepsilon^* A/\mathrm{d}$ (ε_0 is the vacuum permittivity) and taking d $= d$ as the thickness of the dielectric CFO layer. It is clear that at low f the permittivity ε^* values are exceedingly large, thus indicating that nonintrinsic contributions dominate the overall capacitance. In contrast, at high frequencies ε^* is reduced to $\varepsilon^* < 25$, which is a more sound value. Most commonly, a low-f contribution to ε^* comes from Schottky barriers formed at the contact/insulator interface.[30] Under these circumstances, voltage drops at the thin Schottky barrier (typically a few nanometers thick); therefore, in the presence of a leaky bulk contribution (as in the present case; see below) a fake enhancement of the intrinsic permittivity is derived if d is used as the relevant thickness of the dielectric barrier.[31,32] This interpretation is corroborated by the reduction of the low-f capacitance when increasing bias V_{dc} field as shown by data in Fig. 2, where $C(f)$ data collected at $V_{dc} = 0, 0.5$, and 1 V are displayed. Moreover, it is found that for a given CFO film thickness and at low f, the dependence of the capacitance on V_{dc} is $C^{-1} \sim V^{1/2}$ (not shown here) as expected for a Schottky barrier. The observation that at high-f, C (and ε^*) are independent of V_{dc} also signals that the intrinsic behavior dominates in this frequency region. A common way to visualize the existence of distinct contributions in ac-conductivity experiments is by plotting the out-of-phase $Z''(f)$ vs the in-phase component $Z'(f)$ of the frequency-dependent impedance $Z(f)$ as shown in the inset of Fig. 2. The observation of two quasi-circles in the $Z''(Z')$ plot reflects the contribution of two RC-like circuits in the measured sample.[33] Consistently with data in the main panel, the low-frequency contribution is rapidly suppressed by the V_{dc} bias (distinct symbols correspond to V_{dc} as in main panel).

In Fig. 3(a), we show the capacitance measured using Pt and Au electrodes (square and triangle symbols, respectively) at $V_{dc} = 0$. The comparison of both sets of data confirms that the capacitance measured at the low-f region is largely dominated by the CFO-electrode interface. In contrast, the $C(f)$ values for $f > 100$ kHz are independent of the electrode, thus reflecting the intrinsic character. In agreement with discussion of Fig. 2, the equivalent circuit of the sample should contain, at least, two RC-like elements: $(RC)_i$ and $(RC)_b$ representing the interface contribution and the bulk of the film, respectively. $R_x (= G_x^{-1})$ and C_x stand for the dc resistance (conductance) and capacitance of each element ($x = i,b$). The permittivity drop at intermediate frequencies reflects the frequency region where the interface contribution starts to vanish. Moreover, a detailed inspection of the high-f region of $C(f)$ reveals the existence of a weak frequency dependence. This is a common observation in dielectrics and it is associated with an ac-conductivity term (G_{ac}) that accompanies G_b and C_b.[34,35]

This contribution is more clearly seen if the measured conductance is plotted as a function of frequency as shown in Fig. 3 (inset). In this log-log plot, the almost-linear high-f region corresponds to the so-called universal dielectric

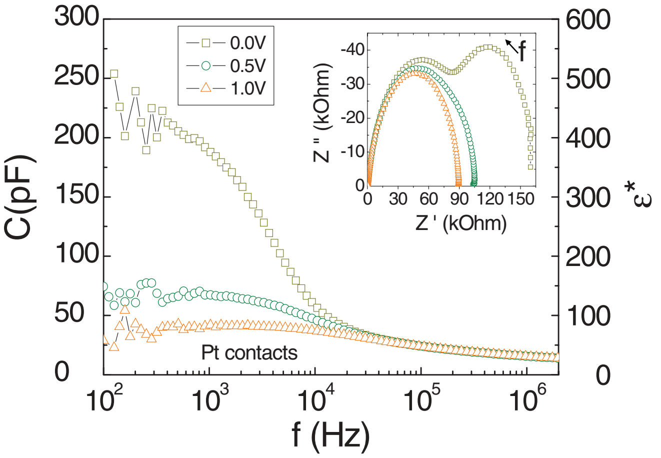

FIG. 2. (Color online) Dependence of the capacitance $C(f)$ and permittivity ε^* on frequency (left and right axis) for a 160-nm-thick CFO film, measured using different applied bias voltages $V_{dc} = 0$, 0.5, and 1.0 V (squares, circles, and triangles, respectively). Inset: Imaginary part (Z'') vs real part (Z') of the impedance Z for the same Pt contact measured under distinct V_{dc} bias.

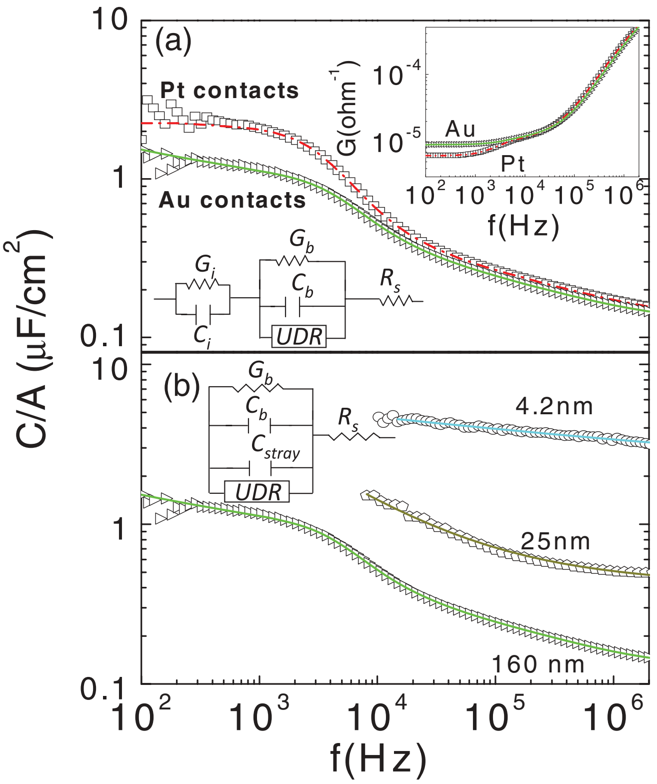

FIG. 3. (Color online) (a) Capacitance vs frequency of a 160-nm-thick CFO film measured using Pt (squares) and Au (triangles) contacts and fits (lines) using the equivalent circuit as shown in the schematic in the lower inset in (a). Upper inset: dependence of the conductance $G(f)$ on the frequency of the same film using Pt and Au contacts as indicated. (b) Frequency dependence of the capacitances of the 160-, 25-, and 4.2-nm-thick CFO films and fits (lines). The film with 160-nm thickness was measured using large contacts and needles, whereas films of 25 and 4.2 nm were measured by using *e*-beam lithographed smaller contacts and the AFM tip as described in the text. Inset in (b): schematic of the equivalent measuring circuit for the AFM tip.

relaxation (UDR) contribution which can be represented by $G_{ac} = G^0_{ac}\omega^S$, where ω is the angular frequency of the driving ac field and S is some power smaller than 1; the UDR accounts for the frequency dependence observed in the high-frequency region of $C(f)$.[34,35] Therefore, the complete equivalent circuit, representing the bulk of the sample, the contact interface, and a series resistance corresponding to the wiring (R_S) is that shown in the sketch in Fig. 3(a).

Using this circuit model, the $C(f)$ and $G(f)$ for the 160-nm sample measured by using either Au or Pt electrodes can be very well fitted as shown by the continuous lines through the data in Fig. 3(a) (main panel and inset). The same circuit model has been used to fit the data for all films. The exceptions are the thinnest films, which as mentioned, had been measured using the AFM tip. In this case, a parallel capacitance (C_{stray}) representing the capacitor formed by the sample and the metallic cantilever must be included as indicated in the equivalent circuit shown in the sketch in Fig. 3(b). C_{stray} has been determined by measuring the capacitance at a given frequency, as a function of the distance (z) between the tip and the sample. Using the slope of $C(z)$ vs z^{-1} and the z value at sample surface, we obtained C_{stray},[36] which is subsequently fixed when fitting $C(f)$. This simple model allows one to obtain good fits of the $C(f)$ as illustrated in Fig. 3(b) where data for the 160, 25, and 4.2 nm CFO films and the corresponding fits (solid lines through data) are shown. We note that for the thinnest films (<60 nm), for which small area electrodes have been used, at $f < 10$ kHz the impedance of the sample/electrode system exceeds the available measuring range of the impedance analyzer and thus data cannot be collected.

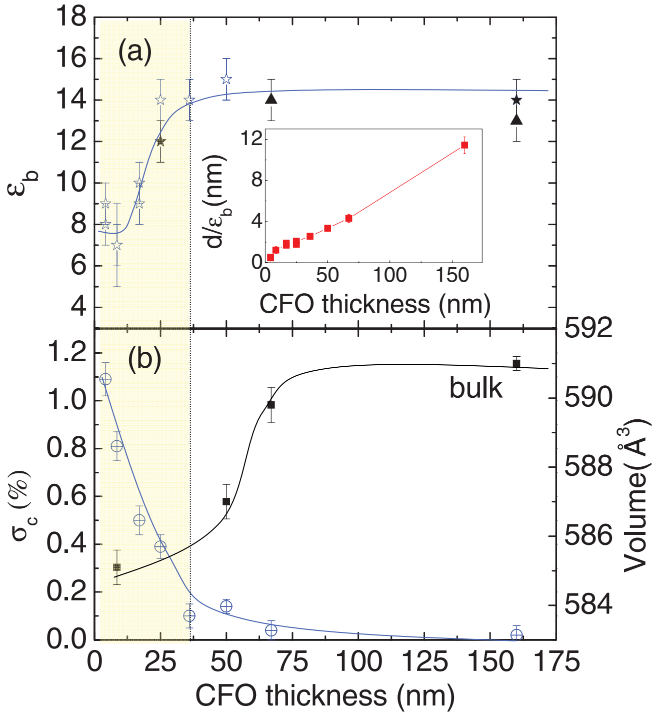

FIG. 4. (Color online) (a) Dependence of the permittivity ε_b of CFO films on thickness. Distinct permittivity ε_b values plotted for a given thickness correspond to results obtained using distinct contacts or different techniques (open stars, AFM tip on Au contacts; open triangle, probe station needles on Au contacts; solid triangles, needles on Pt contacts). Inset: inverse of capacitance (d/ε_b) vs CFO thickness. (b) Out-of-plane strain (circles, left axis) and unit-cell volume (squares, right axis) of CFO films as a function of film thickness.

The fits described above, allow us to extract the parameters of the equivalent circuits for each CFO film. Of relevance here are the permittivity ε_b values (evaluated from C_b) and their thickness dependence collected in Fig. 4(a). In Fig. 4(a) two values of permittivity for a given thickness correspond to results from measurements using distinct contacts and/or using a different technique (AFM tip or needles) as indicated. We first note that for $d > 30$ nm, $\varepsilon_b = \varepsilon_r \approx 14$, where ε_r denotes the relative permittivity of the film. This value is in good agreement with permittivity value reported for bulk CFO ($\varepsilon_r \approx 12$) (Ref. 37) and indicates that ε_r of relaxed CFO films is bulk-like. More interestingly, however, is the observation that for thinner films ($d < 30$ nm) the permittivity decays rather abruptly by about ∼40%; for instance, for $d = 8.5$ nm, $\varepsilon_b \approx 8$. We note that if the permittivity data is plotted as d/ε_b vs d, as typically done to evidence the presence of dead layers in ferroelectric capacitors,[30] it turns out that data for

$d > 30$ follows a straight line [see inset in Fig. 4(a)] that extrapolates to $d = 0$ thus excluding that a dead layer, at least one of constant thickness, could be responsible for the observed variation of permittivity. We strengthen that, to our knowledge, a systematic measurement of permittivity of CFO epitaxial thin films had not been reported earlier.

To get some insight into the microscopic mechanism of the observed reduction of permittivity, we show in Fig. 4(b) the measured variation of the strain along the c axis ($\sigma_c = [c(d) - c_0]/c_0$, where $c(d)$ and c_0 are the out-of-plane cell parameters of the films and bulk CFO, respectively) resulting from the epitaxial compressive in-plane strain. It follows from data in Fig. 4(b) that the strain observed in the thinnest films, is rapidly reduced for $d > 30$ nm. Therefore, from the comparison of data in Figs. 4(a) and 4(b), a direct connection between the decrease of the permittivity and the expansion of the c axis, can be clearly appreciated. However, the effect of the in-plane compressive strain on the c-axis permittivity of CFO films is at odds with expectations based on simple grounds; that is, a c-axis expansion should be accompanied by an enhancement of the corresponding permittivity due to the enlargement of the ionic bonds along that axis. Indeed, this is the observed behavior of some perovskite oxides, such as $SrTiO_3$, where it has been shown that compressive strain increases permittivity, eventually promoting the occurrence of a polar state.[19] Therefore, the observed reduction of c-axis permittivity cannot be simply explained on the basis of the c-axis variation resulting from the compressive in-plane epitaxial strain.

However, some recent reports on structural data and Raman spectroscopy of strained CFO could be inspiring. Indeed, it has been shown by Raman spectroscopy that in compressively strained CFO films grown on $MgAl_2O_4$ and $SrTiO_3$ substrates[9,10] phonon modes shift to higher frequencies upon strain-induced c-axis expansion. This striking observation was rationalized by noticing that the measured overall unit-cell volume compression is the dominating factor, thus explaining the observed Raman blueshift. The structural data shown in Fig. 1 also follows the same trend; that is, the CFO unit-cell volume V_{CFO}, determined using measured in-plane and out-of-plane cell parameters of CFO films [Fig. 4(b) (solid squares, right axis)] clearly reduces when increasing compressive strain. Therefore, from the data in Fig. 4 it can be argued that the permittivity decreases when increasing compressive epitaxial strain as a result of the reduction of the unit-cell volume, thus mimicking the results of Raman spectroscopy.[9,10] The reduction of permittivity upon reducing the unit-cell volume is in agreement with results reported in related oxides under hydrostatic pressure (P).[39,40] For MgO, for instance, $d \ln \varepsilon / dP \approx -0.3 \times 10^{-5}$ bar^{-1}.[37,38] In the particular case of the CFO films described here, $d \ln \varepsilon / dP$ can be estimated by using $d \ln \varepsilon / dP = (d \ln \varepsilon / d \ln V)/B$, where B is the bulk modulus. By using $B \approx 200$ GPa as reported for CFO (Ref. 38) and ($d \ln \varepsilon / d \ln V$) from Fig. 4(b), we obtain $d \ln \varepsilon / dP \approx -3 \times 10^{-5}$ bar^{-1}. It thus follows that although the observed reduction of permittivity is in agreement with the expected trend upon unit volume compression, the measured variation is about one order of magnitude larger than the one found for oxides having rocksalt structure. As it could be argued that the more open structure of spinels could lead to a larger $d \ln \varepsilon / d \ln V$ variation, deeper insight is required.

TABLE I. Calculated values of the permittivity tensor. The upper row is calculated for the experimental lattice constants, whereas the lower rows correspond to theoretical lattice constants and strained configurations relative to the latter. $\varepsilon_{x/y}$ and ε_z correspond to the in-plane (a) and out-of-plane (c) directions, respectively, whereas $\langle\varepsilon\rangle$ is averaged over all three Cartesian directions. Columns denoted "Elect." and "Ion." list the electronic (ε_∞) and ionic (phonon) contributions, respectively, to the dielectric constant. $\langle\varepsilon_{\mathrm{tot}}\rangle$ is the total dielectric constant averaged over all three Cartesian directions.

			Elect.	Ion.	Elect.	Ion.	Elect.	Ion.	
a_0 (Å)	a/a_0	c/c_0	$\varepsilon_{x/y}$		ε_z		$\langle\varepsilon\rangle$		$\langle\varepsilon\rangle_{\mathrm{tot}}$
8.392	1.00	1.00	7.62	8.31	7.56	8.74	7.60	8.45	16.05
8.464	1.00	1.00	7.52	8.94	7.44	9.54	7.50	9.14	16.64
8.464	0.99	1.0113	7.55	8.37	7.54	10.01	7.55	8.92	16.46
8.464	0.98	1.00	7.69	7.81	7.72	8.77	7.70	8.13	15.83

To obtain a better understanding of strain effects on the dielectric properties of spinel films and aiming to disentangle the mechanisms for the observed reduction in permittivity, we performed first-principles calculations of the dielectric tensor under different epitaxial strain conditions. We follow the approach of Refs. 26 and 27 and represent the inverse spinel structure of CFO using a fully ordered cation arrangement with $P4_122$ space group symmetry. This configuration has the lowest total energy relative to other likely high-symmetry configurations[26] and recent Raman studies have suggested short-range order of this type both in $NiFe_2O_4$ thin films and in the bulk.[9,40] We have also performed test calculations for other cation arrangements, which lead to very similar results. The calculated permittivity values are listed in Table I. It can be seen that the calculated permittivity averaged over all three Cartesian directions is very close to the value measured for the thicker, i.e., bulk-like films. Due to the slight overestimation of the lattice constant within the GGA + U approach,[27,41] the permittivity calculated at the theoretical equilibrium volume is slightly larger than the one calculated at the experimental lattice constant. This is consistent with the simple expectation that larger volume leads to softer phonon modes. Indeed, the increase of the calculated permittivity is due to the increase of the ionic contribution to ε, whereas the electronic contribution (ε_∞) is in fact decreasing slightly (due to a small increase in the band gap). If the lattice constants in the x-y plane are compressed by -1%, to simulate the effect of epitaxial strain, the "out-of-plane" lattice constant along the z direction expands by $+1.13\%$.[27,41] This leads to a reduction of the in-plane permittivity by -0.54 and an increase of the c-axis permittivity by $+0.57$. This is again in agreement with the simple expectation described in the previous paragraph, but it is at odds with the experimental observations. As discussed in Ref. 10 the observed out-of-plane relaxation in the CFO films is much weaker than what would be expected both from the calculated two-dimensional Poisson ratio and from the measured bulk elastic constants. The reason for this is currently unclear. To assess the effect of different out-of-plane strain on the permittivity, we also calculate the permittivity for a compressive in-plane strain of -2% while keeping the out-of-plane lattice parameter fixed to the theoretical bulk value, i.e., we completely suppress any out-of-plane relaxation. It can be seen from Table I that in this case the permittivity along the z direction is indeed reduced by -0.49. This shows that the permittivity along a certain direction is not only affected by the strain along the same direction but also by strain in the perpendicular directions and by the overall change in volume. This is consistent with the fact that not all nearest-neighbor bonds within the spinel structure are oriented parallel to the Cartesian axes and thus the corresponding bond lengths and force constants depend on the global strain state of the structure. However, while the calculated change in permittivity for suppressed c-axis expansion agrees qualitatively with the observed reduction in the thinner CFO films, there is a clear quantitative discrepancy, since the calculated strain-induced changes in ε are significantly smaller than the ones observed experimentally. As density functional theory (DFT) calculations incorporate all characteristic features of the spinel structure, namely, its open character, as far as can be described by the used $P4_122$ space group, it follows that other factors, which are currently not included in the first-principles calculation, are responsible for the strongly reduced permittivity in the thinner films. Such factors could involve strain-induced changes in stoichiometry,[42,43] defect concentration, microstructural features of the films, and a thickness-dependent depletion layer in CFO.

V. SUMMARY AND CONCLUSIONS

In summary, we have reported a systematic study of the effect of epitaxial strain on the dielectric properties of spinel ($CoFe_2O_4$) thin films. We have shown that CFO films on $SrTiO_3//La_{2/3}Sr_{1/3}MnO_3$, when grown strain-free, have a dielectric permittivity ($\varepsilon_b \approx 14$) similar to the one reported for bulk materials. Interestingly, we have observed that the permittivity is largely reduced when increasing the in-plane compressive strain. We have argued that this remarkable effect can be qualitatively described as resulting from the unit-cell volume reduction under epitaxial compressive strain. We performed DFT calculation of epitaxial strain effects on dielectric permittivity. It has been found that there is a competition between a permittivity enhancement along the out-of-plane direction due to its strain-induced expansion and a reduction of overall permittivity due to the shrinking of the CFO unit-cell volume under compressive strain. The DFT calculations and estimates based on available elastic constants both predict a reduction of permittivity with increasing compressive strain if the out-of-plane expansion along c is suppressed, as observed. However, the measured variation appears to be about one order of magnitude larger than predicted, thus indicating that other effects, such as plastic defects or changes of stoichiometry of the film either as a response to elastic strain (as typically found in perovskites) or due to the growth should be considered. Possibly, the open structure of spinel oxides, allowing more complex patterns of lattice deformations under compressive strain and eventually modifying the film symmetry, may also play an important role.

ACKNOWLEDGMENTS

Financial support by the Spanish Government (Projects MAT2011-29269-C03 and CSD2007-00041) and Generalitat de Catalunya (2009 SGR 00376) is acknowledged. We thank F. Sánchez and N. Dix for their knowledge and help on thin-film growth and Miquel Rubio for his assistance on e-beam lithography.

---

[*] Present address: Institut für Physik, Johannes Gutenberg-Universität Mainz, Staudinger Weg 7, 55099 Mainz, Germany.

[1] A. Krimmel, A. Loidl, M. Klemm, S. Horn, and H. Schober, Phys. Rev. Lett. **82**, 2919 (1999).

[2] Y. Yamasaki, S. Miyasaka, Y. Kaneko, J. P. He, T. Arima, and Y. Tokura, Phys. Rev. Lett. **96**, 207204 (2006).

[3] M. Alexe, M. Siese, D. Hesse, P. Esquinazi, K. Yamahuchi, T. Fukushima, S. Picozzi, and U. Gösele, Adv. Mater. **44**, 4452 (2009).

[4] J. Hemberger, H. A. Krug von Nidda, V. Tsurkan, and A. Loidl, Phys. Rev. Lett. **98**, 147203 (2007).

[5] U. Lüders, A. Barthélémy, M. Bibes, K. Bouzehouane, S. Fusil, E. Jacquet, J. P. Contour, J.-F. Bobo, J. Fontcuberta, and A. Fert, Adv. Mater. **18**, 1733 (2006); U. Lüders, M. Bibes, K. Bouzehouane, E. Jacquet, J. P. Contour, S. Fusil, J. F. Bobo, J. Fontcuberta, A. Barthélémy, and A. Fert, Appl. Phys. Lett. **88**, 082505 (2006).

[6] A. V. Ramos, M. J. Guittet, J. B. Moussy, R. Mattana, C. Deranlot, F. Petroff, and C. Gatel, Appl. Phys. Lett. **91**, 122107 (2007).

[7] F. Rigato, S. Piano, M. Foerster, F. Giubileo, A. M. Cucolo, and J. Fontcuberta, Phys. Rev. B **81**, 174415 (2010).

[8] M. Gajek, M. Bibes, S. Fusil, K. Bouzehouane, J. Fontcuberta, A. Barthélémy, and A. Fert, Nature Mater. **6**, 296 (2007).

[9] M. N. Iliev, D. Mazumdar, J. X. Ma, A. Gupta, F. Rigato, and J. Fontcuberta, Phys Rev. B **83**, 014108 (2011).

[10] M. Foerster, M. Iliev, N. Dix, X. Martí, M. Barchuk, F. Sánchez, and J. Fontcuberta, Adv. Funct. Mater. (2012), doi: 10.1002/adfm.201200257.

[11] Y. Suzuki, Annu. Rev. Mater. Res. **31**, 265 (2001).

[12] W. Huang, L. X. Zhou, H. Z. Zeng, X. H. Wei, J. Zhu, Y. Zhang, and Y. R. Li, J. Cryst. Growth **300**, 426 (2007).

[13] M. Foerster, J. M. Rebled, S. Estradé, F. Sánchez, F. Peiró, and J. Fontcuberta, Phys. Rev. B **84**, 144422 (2011).

[14] A. Lisfi, C. M. Williams, L. T. Nguyen, J. C. Lodder, A. Coleman, H. Corcoran, A. Johnson, P. Chang, A. Kumar, and W. Morgan, Phys. Rev. B **76**, 054405 (2007).

[15] M. Pan, G. Bai, Y. Liu, S. Hong, V. P. Dravid, and A. K. Petford-Long, J. Appl. Phys. **107**, 043908 (2010).

[16] J. A. Moyer, C. A. F. Vaz, E. Negusse, D. A. Arena, and V. E. Henrich, Phys. Rev. B **83**, 035121 (2011).

[17] P. D. Thang, G. Rijnders, and D. H. A. Blank, J. Magn. Magn. Mater. **310**, 2621 (2007).

[18] L. Horng, G. Chern, M. C. Chen, P. C. Kanga, and D.S. Leeb, J. Magn. Magn. Mater. **270**, 389 (2004).

[19] J. H. Haeni, P. Irvin, W. Chang, R. Uecker, P. Reiche, Y. L. Li, S. Choudhory, W. Tian, M. E. Hawley, B. Craigo, A. K. Tagantsev,

X. Q. Pan, S. K. Streiffer, L. Q. Chen, S. W. Kirchoefer, J. Levi, and D. G. Schlom, Nature (London) **430**, 758 (2004).

[20] I. C. Infante, F. Sánchez, J. Fontcuberta, M. Wojcik, E. Jedryka, S. Estradé, F. Peiro, J. Arbiol, V. Laukhin, and J. P. Espinos, Phys. Rev. B **76**, 224415 (2007).

[21] J. H. Lee, L. Fang, E. Vlahos, X. Ke,Y. W. Jung, L. F. Kourkoutis, J. Kim, P. J. Ryan, T. Heeg, M. Roeckerath, V. Goian, M. Bernhagen, R. Uecker, P. C. Hammel, K. M. Rabe, S. Kamba, J. Schubert, J. W. Freeland, D. A. Muller, C. J. Fennie, P. Schiffer, V. Gopalan, E. J. Halperin, and D. G. Schlom, Nature (London) **466**, 954 (2010).

[22] J. Fontcuberta, I. Fina, L. Fàbrega, F. Sánchez, X. Martí, and V. Skumryev, Phase Transitions **84**, 555 (2011).

[23] W. Chen and W. Zhu, J. Am. Ceram. Soc. **94**, 1096 (2011).

[24] M. Gajdoš, K. Hummer, G. Kresse, J. Furthmüller, and F. Bechstedt, Phys. Rev. B **73**, 045112 (2006).

[25] G. Kresse and J. Furthmüller, Comput. Mater. Sci. **6**, 15 (1996).

[26] D. Fritsch and C. Ederer, Appl. Phys. Lett. **99**, 081916 (2011).

[27] D. Fritsch and C. Ederer, Phys. Rev. B **86**, 014406 (2012).

[28] J. P. Perdew, K. Burke, and M. Ernzerhof, Phys. Rev. Lett. **77**, 3865 (1996).

[29] V. I. Anisimov, F. Aryatesiawan, and A. I. Lichtenstein, J. Phys.: Condens. Matter **9**, 767 (1997).

[30] L. Pintilie, I. Vrejoiu, D. Hesse, G. LeRhun, and M. Alexe, Phys. Rev. B **75**, 224113 (2007).

[31] P. Lunkenheimer, V. Bobnar, A. V. Pronin, A. I. Ritus, A. A. Volkov, and A. Loidl, Phys. Rev. B **66**, 052105 (2002).

[32] P. Lunkenheimer, S. Krohns, S. Riegg, S. G. Ebbinghaus, A. Reller, and A. Loidl, Eur. Phys. J. Spec. Top. **180**, 61 (2010).

[33] N. Hirose and A. R. West, J. Am. Ceram. Soc. **79**, 1633 (1996).

[34] A. K. Jonscher, Nature (London) **267**, 673 (1977).

[35] A. K. Jonscher, J. Phys. D: Appl. Phys. **32**, 57 (1999).

[36] In the experimental conditions used, $C_{\text{stray}} \approx 0.25$ pF.

[37] M. I. Danilkevuich and I. I. Makoed, Phys. Status Solidi B **222**, 541 (2000).

[38] F. Seitz, Phys. Rev. **79**, 372 (1950).

[39] A. J. Bosman and E. E. Havinga, Phys. Rev. **129**, 1593 (1963).

[40] V. G. Ivanov, M. V. Abrashev, M. N. Iliev, M. M. Gospodinov, J. Meen, and M. I. Aroyo, Phys. Rev. B **82**, 024104 (2010).

[41] D. Fritsch and C. Ederer, Phys. Rev. B **82**, 104117 (2010).

[42] S. Estradé, J. Arbiol, F. Peiró, I. C. Infante, F. Sánchez, J. Fontcuberta, F. de la Peña, M. Walls, and C. Colliex, Appl. Phys. Lett. **93**, 112505 (2008).

[43] S. Estradé, J. M. Rebled, J. Arbiol, F. Peiró, I. C. Infante, G. Herranz, F. Sánchez, J. Fontcuberta, R. Córdoba, B. G. Mendis, and A. L. Bleloch, Appl. Phys. Lett. **95**, 072507 (2009).